Supplemental Data

Table S1: Reciprocal crosses

Cross	*lrx8-/- lrx9-/- lrx10-/+* **X** *Col*	Col **X** *lrx8-/- lrx9-/- lrx10-/+*	*lrx8-/- lrx9-/- lrx11-/+* **X** *Col*	Col **X** *lrx8-/- lrx9-/- lrx11-/+*
F1	*lrx10-/+* = 29	*lrx10-/+* = 8	*lrx11-/+* = 31	*lrx11-/+* = 9
TE	96.7%	26.7%	103.3%	30%
Chi^2 P-value	1	0.0001	1	0.0001
Cross	*lrx8-/- lrx9-/- lrx10-/+ lrx11-/-* **X** *Col*	Col **X** *lrx8-/- lrx9-/- lrx10-/+ lrx11-/-*	*lrx8-/- lrx9-/- lrx10-/- lrx11-/+* **X** *Col*	Col **X** *lrx8-/- lrx9-/- lrx10-/- lrx11-/+*
F1	*lrx10-/+* = 30	*lrx10-/+* = 12	*lrx11-/+* = 27	*lrx11-/+* = 9
TE	100	40	90	30
Chi^2 P-value	1	0.001	0.7	0.0001

Crosses (female X male); F1 = 60 plants; TE = Transmission efficiency

Table S2: List of Primers

Target Sequence	**Primer**	**Sequence**
LRX8	**Lrx8 F1**	GAGATTGTGTTTATTGGGAACAAC
	Lrx8 R1	ATGGTGTCTCAGGCTTTGGACTAG
LRX9	**Lrx9 F1**	AAGATACAACGAATTTGAAGGAAG
	Lrx9 R1	TTCTTCCGGTTTAGGAGATTCATG
LRX10	T.Lrx10 F1	GTTTGTTCTCCGGATGTGAAGCT
	Lrx10 R1	GGTTGTGGTTTATGAACTGGCCTA
LRX11	**Lrx11 F3**	TACCTTAGGGAGGTATCTTGCAG
	Lrx 11 R	ATCGAATTCGTGCATTAGCTTTAGC
	LBb1.3	ATTTTGCCGATTTCGGAAC
***LRX8* frgt1**	LRX8 proF1	CTGCAGTTGGCCTCATTAAAGTTAGTAGTTCC
	LRX8 terR1	GTCGACTCAAATCTATTGTTGTTCAAGAAGATG
***LRX8* frgt2**	LRX8 proF2	GTCGACCATCCCCGAGACAATTGGTAA
	LRX8 terR2	TCTAGAAAGTACCGAGACTTTTCCTCGTTG
5' qRT_LRX8	5'qRTLRX8_F1	GCGGGGATTGACCTTAACCA
	5'qRTLRX8_R1	GAAACGGACCAACGAAACGG
3' qRT_LRX8	3'qRTLRX8_F1	TCACCAAAACCAACACCAACAC
	3'qRTLRX8_R1	ACTCTGGCTTAGGTTCCTTTGG
5' qRT_LRX9	5'qRTLRX9_F1	ATACCGTCGTTGCCACCTTT
	5'qRTLRX9_R1	AACCAACCCAATTGGCCGTA
3' qRT_LRX9	3'qRTLRX9_F1	GTGGTTAGTCGTCCTGTGGATT
	3'qRTLRX9_R1	GTGTTTTTGGTGTCTCGGGTTT
5' qRT_LRX10	5'qRTLRX10_F1	CTACCATTCCTGATTCCCTCGG
	5'qRTLRX10_R1	GAGGTAGAACACCAGTGAAGG
3' qRT_LRX10	3'qRTLRX10_F1	CTACACCGTCGAAGTCTCCATC
	3'qRTLRX10_R1	GAATGGACTGGTGGTGAGGTAG
5' qRT_LRX11	5'qRTLRX11_F1	CTAACCGATACAGAAGCTGCCT
	5'qRTLRX11_R1	CCTTTTTCCAAGCCTGAAGAGC
3' qRT_LRX11	3'qRTLRX11_F1	ACGAGCGTGGAGGAAATTGATA
	3'qRTLRX11_R1	GTGTGTCATCCAACGCAATCTC
LRR11	Lrx11 proF	CCTTGAGTCAACACTGCACTGG
	Lrx11_oE_F	AGACTCGAGATGCCCTTCTATAAGCAGCC
	Lrx11 PstIR	CTGCAGCAAGGACAAGTGCGCTGGTGGCTC
EXT11	Lrx11 PstIF	CTGCAGTCAACCGGGCGGTTGATC
	Lrx11 terR	TACACAAGCCCATTATTAGGCC

***LRX11* terminator**	PstI 11TF	CCTGCAGTGATCTCAATCGAAGAGAG
	NotI 11TR-1	TGCGGCCGCTACACAAGCCCATTATTAGG
Citrine1	T.Cit F_PstI	CTGCAGCATGGTGAGCAAGGGCGAGGAG
	Cit_R_PstI	GCTGCAGCTTGTACAGCTCGTCCATG
	T.Cit R_PstI	GCTGCAGCTACTTGTACAGCTCGTCCATG
Citrine2	T.Cit-F	CTGCAGCATGGTGAGCAAGGGCGAGGAG
	T.Cit-R_SpeI	TACTAGTCTACTTGTACAGCTCGTCCATG
	NotI Subclone	TCGAGACTGGCGGCCGCCAGTC
	SpeI Subclone	CTAGCTAGACATGCATGTCTAG
Vector + proACT1	TNF001	CATGAGATCTTTTCTTCTACCTTTATGCAAAACC
	TNF004	CCTGAGATCTCCGATCTAGTAACATAGATG
nlsR$_m$-2A-secG$_f$	TNF002	AAAAGGATCCCCACCATGGCTCCTAAGAAAAAGAGAAAGG
	TNF003	TTTTGGATCCTTACTTATCGTCATCATCCT

Underlined sequences correspond to introduced restriction sites. frgt = fragment. The sequence in red/bold are used along with the LBb1.3 primer for T-DNA amplification of mutant alleles. The *Not*I subclone and *Spe*I subclone were used to introduce *Not*I and *Spe*I sites into the *pSC* vector, respectively.

Movies

Movie S1: *lrx8/9/11* pollen in liquid PGM showing high frequency of bursting during imbibition

Movie S2: Growing *lrx8/9/11* PT labelled with FM1-43 showing intermittent growth and the discharge of cytoplasmic membrane-stained components.

Movie S3: Growing *lrx8/9/11* PT labelled with FM1-43 showing vesicle budding.

Figures

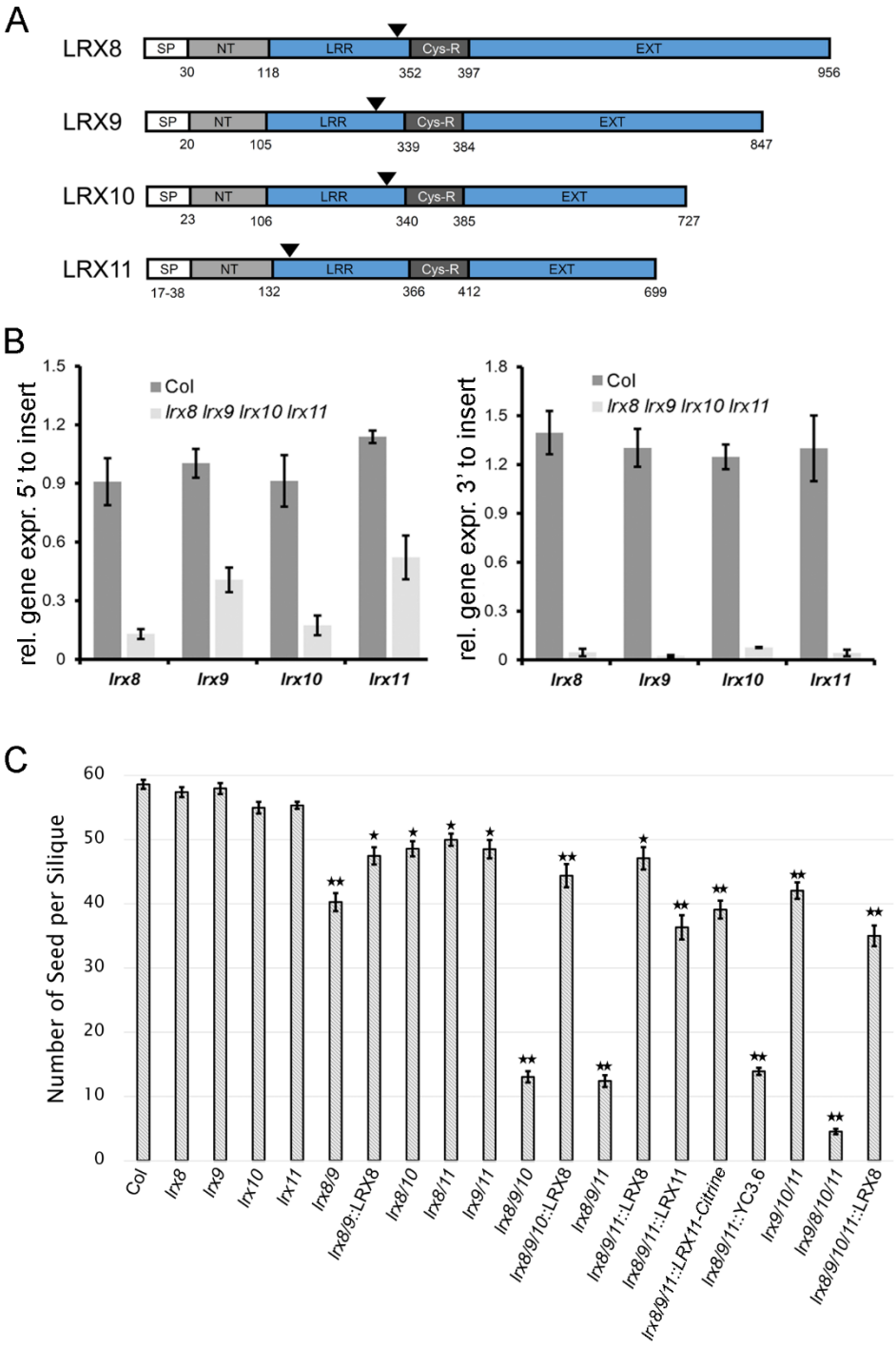

Figure S1: LRX protein structures and effects of mutations on seed set. A. Schematic representation of the LRX8, LRX9, LRX10 and LRX11 proteins. NT: N-terminal domain preceding the LRR domain; LRR: Leucine-rich repeat domain; Cys-R: Cys-rich hinge region; EXT: extensin domain. For sequence comparison, see Figure

S2. For T-DNA insertion sites, the corresponding position in the protein and the amino acid residues are indicated; *lrx8*: 340, *lrx9*: 301; *lrx10*: 312; *lrx11*: 137. **B.** Quantitative RT-PCR on total RNA extracted from open flowers. Coding sequences 5' upstream (left graph) and 3' downstream (right graph) of the insertion sites were amplified. Each data point represents technical triplicates for each of biological quadruplicates. While mRNA of the 5' regions is reduced but still detectable for all the *lrx* genes, mRNA of the 3' region is strongly reduced compared to the wild type. All differences between wild type and quadruple mutant are significantly different (t-test, $p<0.01$) Error bars = s.e.m.. **C.** Plot of the average number of seeds per silique in the wild-type and different mutants (mutant background and gene used for complementation are separated by a double colon). Statistical differences compared to the wild type are shown, t-test, * = $p < 0.01$, ** = $p < 0.0001$, $n \geq 48$, error bars = s.e.m..

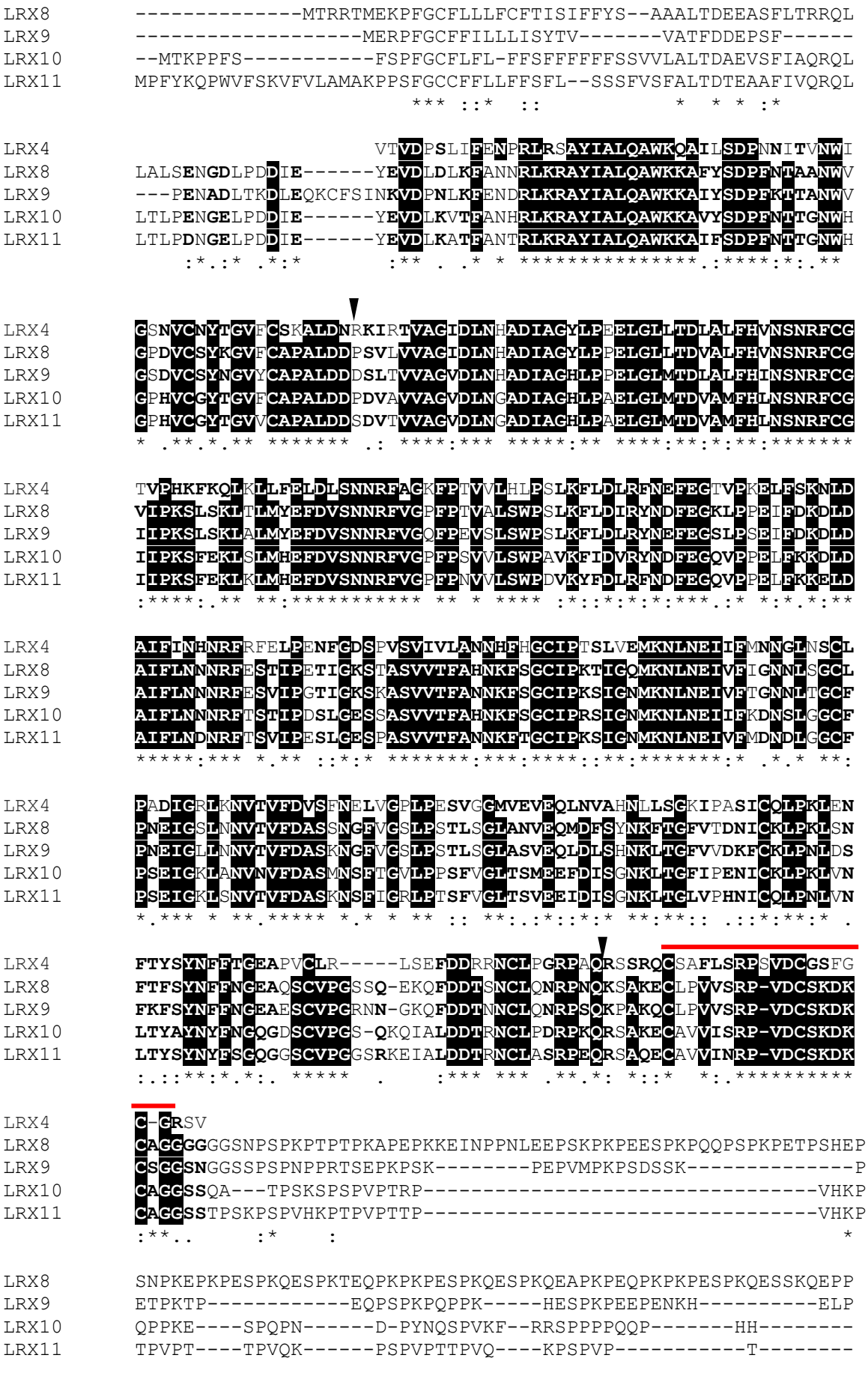
LRX8 ----------MTRRTMEKPFGCFLLLFCFTISIFFYS--AAALTDEEASFLTRRQL
LRX9 ----------MERPFGCFFILLLISYTV-------VATFDDEPSF------
LRX10 --MTKPPFS----------FSPFGCFLFL-FFSFFFFFSSVVLALTDAEVSFIAQRQL
LRX11 MPFYKQPWVFSKVFVLAMAKPPSFGCCFFLLFFSFL--SSSFVSFALTDTEAAFIVQRQL
LRX4 VTVDPSLIFENPRLRSAYIALQAWKQAILSDPNNITVNWI
LRX8 LALSENGDLPDDIE------YEVDLDLKFANNRLKRAYIALQAWKKAFYSDPFNTAANWV
LRX9 ---PENADLTKDLEQKCFSINKVDPNLKFENDRLKRAYIALQAWKKAIYSDPFKTTANWV
LRX10 LTLPENGELPDDIE------YEVDLKVTFANHRLKRAYIALQAWKKAVYSDPFNTTGNWH
LRX11 LTLPDNGELPDDIE------YEVDLKATFANTRLKRAYIALQAWKKAIFSDPFNTTGNWH
LRX4 GSNVCNYTGVFCSKALDNRKIRTVAGIDLNHADIAGYLPEELGLLTDLALFHVNSNRFCG
LRX8 GPDVCSYKGVFCAPALDDPSVLVVAGIDLNHADIAGYLPPELGLLTDVALFHVNSNRFCG
LRX9 GSDVCSYNGVYCAPALDDDSLTVVAGVDLNHADIAGHLPPELGLMTDLALFHINSNRFCG
LRX10 GPHVCGYTGVFCAPALDDPDVAVVAGVDLNGADIAGHLPAELGLMTDVAMFHLNSNRFCG
LRX11 GPHVCGYTGVVCAPALDDSDVTVVAGVDLNGADIAGHLPAELGLMTDVAMFHLNSNRFCG
LRX4 TVPHKFKQLKLLFELDLSNNRFAGKFPTVVLHLPSLKFLDLRFNEFEGTVPKELFSKNLD
LRX8 VIPKSLSKLTLMYEFDVSNNRFVGPFPTVALSWPSLKFLDIRYNDFEGKLPPEIFDKDLD
LRX9 IIPKSLSKLALMYEFDVSNNRFVGQFPEVSLSWPSLKFLDLRYNEFEGSLPSEIFDKDLD
LRX10 IIPKSFEKLSLMHEFDVSNNRFVGPFPSVVLSWPAVKFIDVRYNDFEGQVPPELFKKDLD
LRX11 IIPKSFEKLKLMHEFDVSNNRFVGPFPNVVLSWPDVKYFDLRFNDFEGQVPPELFKKELD
LRX4 AIFINHNRFRFELPENFGDSPVSVIVLANNHFHGCIPTSLVEMKNLNEIIFMNNGLNSCL
LRX8 AIFLNNNRFESTIPETIGKSTASVVTFAHNKFSGCIPKTIGQMKNLNEIVFIGNNLSGCL
LRX9 AIFLNNNRFESVIPGTIGKSKASVVTFANNKFSGCIPKSIGNMKNLNEIVFTGNNLTGCF
LRX10 AIFLNNNRFTSTIPDSLGESSASVVTFAHNKFSGCIPRSIGNMKNLNEIIFKDNSLGGCF
LRX11 AIFLNDNRFTSVIPESLGESPASVVTFANNKFTGCIPKSIGNMKNLNEIVFMDNDLGGCF
LRX4 PADIGRLKNVTVFDVSFNELVGPLPESVGGMVEVEQLNVAHNLLSGKIPASICQLPKLEN
LRX8 PNEIGSLNNVTVFDASSNGFVGSLPSTLSGLANVEQMDFSYNKFTGFVTDNICKLPKLSN
LRX9 PNEIGLLNNVTVFDASKNGFVGSLPSTLSGLASVEQLDLSHNKLTGFVVDKFCKLPNLDS
LRX10 PSEIGKLANVNVFDASMNSFTGVLPPSFVGLTSMEEFDISGNKLTGFIPENICKLPKLVN
LRX11 PSEIGKLSNVTVFDASKNSFIGRLPTSFVGLTSVEEIDISGNKLTGLVPHNICQLPNLVN
LRX4 FTYSYNFFTGEAPVCLR-----LSEFDDRRNCLPGRPAQRSSRQCSAFLSRPSVDCGSFG
LRX8 FTFSYNFFNGEAQSCVPGSSQ-EKQFDDTSNCLQNRPNQKSAKECLPVVSRP-VDCSKDK
LRX9 FKFSYNFFNGEAESCVPGRNN-GKQFDDTNNCLQNRPSQKPAKQCLPVVSRP-VDCSKDK
LRX10 LTYAYNYFNGQGDSCVPGS-QKQIALDDTRNCLPDRPKQRSAKECAVVISRP-VDCSKDK
LRX11 LTYSYNYFSGQGGSCVPGGSRKEIALDDTRNCLASRPEQRSAQECAVVINRP-VDCSKDK
LRX4 C-GRSV
LRX8 CAGGGGGGSNPSPKPTPTPKAPEPKKEINPPNLEEPSKPKPEESPKPQQPSPKPETPSHEP
LRX9 CSGGSNGGSSPSPNPPRTSEPKPSK--------PEPVMPKPSDSSK--------------P
LRX10 CAGGSSQA---TPSKSPSPVPTRP----------------------------------VHKP
LRX11 CAGGSSTPSKPSPVHKPTPVPTTP----------------------------------VHKP
LRX8 SNPKEPKPESPKQESPKTEQPKPKPESPKQESPKQEAPKPEQPKPKPESPKQESSKQEPP
LRX9 ETPKTP----------EQPSPKPQPPK-----HESPKPEEPENKH----------ELP
LRX10 QPPKE----SPQPN------D-PYNQSPVKF--RRSPPPPQQP-------HH--------
LRX11 TPVPT----TPVQK------PSPVPTTPVQ----KPSPVP----------T--------

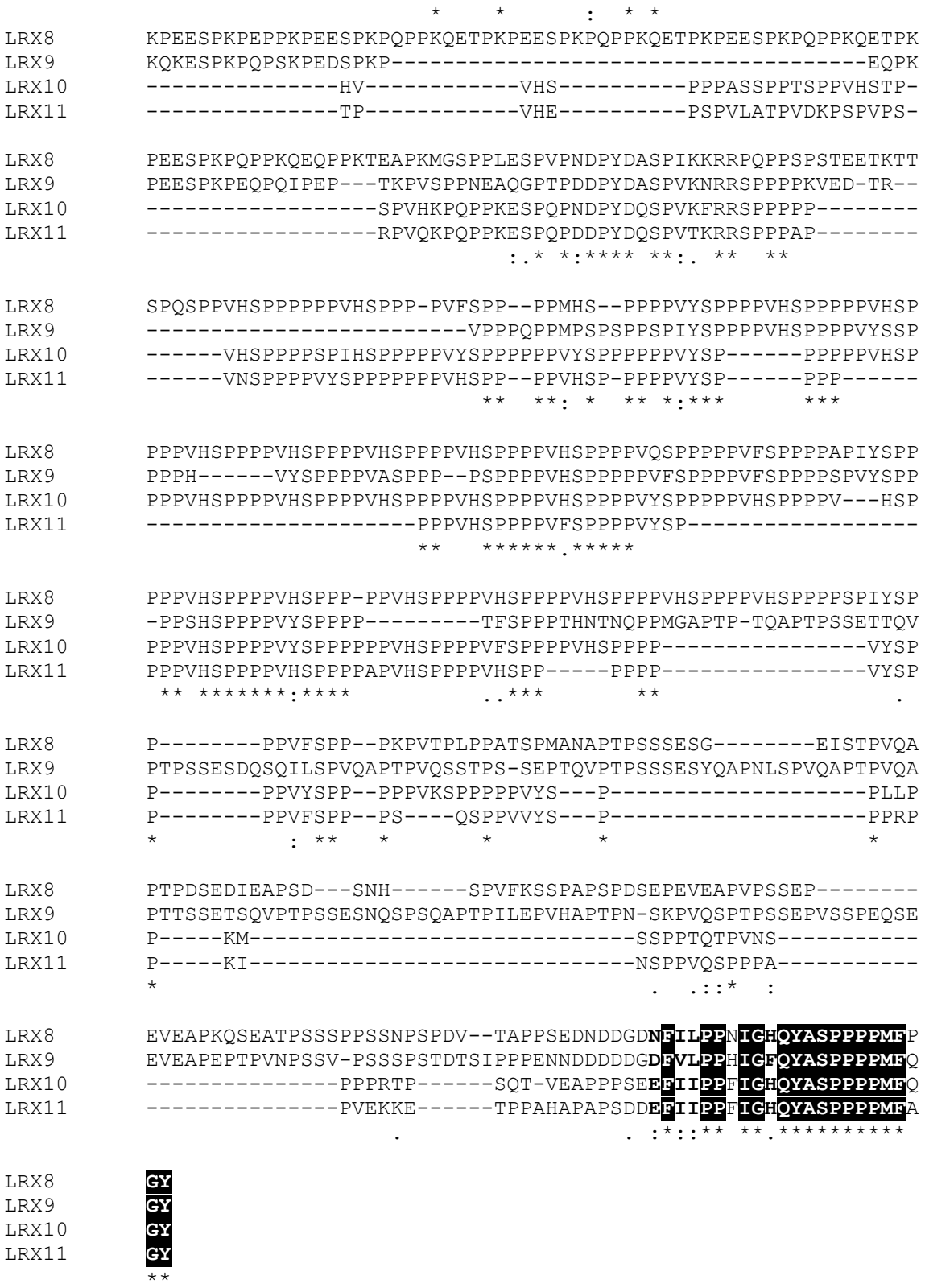

Figure S2: Alignment of LRX8, LRX9, LRX10, LRX11, and LRX4. Alignment was performed using the Clustal O(1.2.4) software. Identical positions are indicated in

black, conserved and similar positions are indicated in grey. The asterisks, colons, and single dots refer to identical, conserved, and similar positions in LRX8-LRX11 only. The LRR domain is delimited by arrowheads and linked to the extensin domain by the conserved Cys-rich hinge domain (indicated with a red line). The extensin domain is characterized by repetitive, sequences rich in the (S-P4)n motif, but is diverse among the proteins, except the last 20 residues that are again highly conserved. For LRX4, only sequences of the N-terminal half are shown that reveal conservation among LRX proteins, i.e. from the end of the signal peptide to the Cys-rich hinge region.

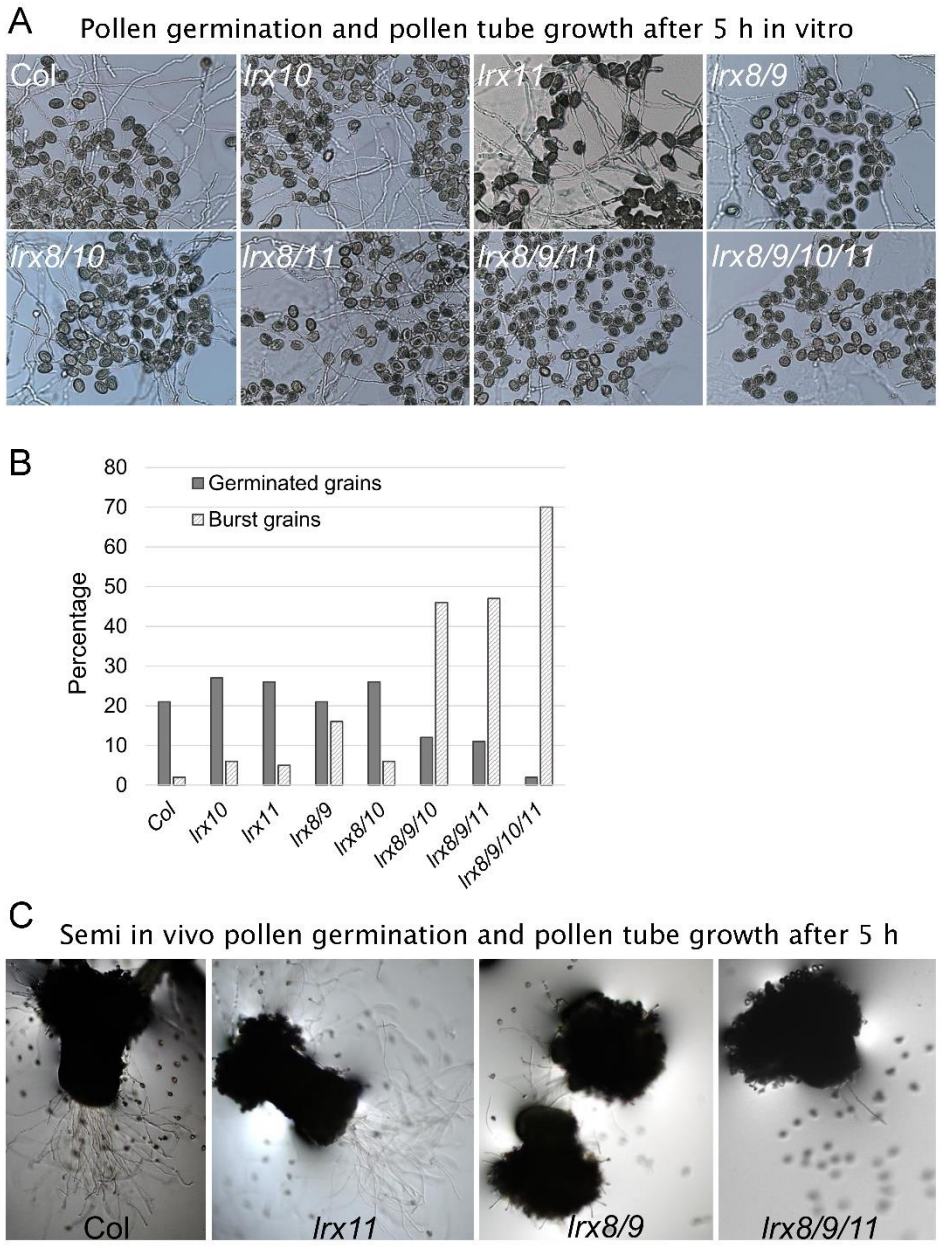

Figure S3: *In vitro* and semi *in vivo* pollen germination after 5 h incubation. A. Representation of pollen germination in the wild type and different *lrx* mutants. Lower germination and higher frequency of PG bursting were observed in the *lrx8/9*, *lrx8/9/11*, and *lrx8/9/10/11* mutants. **B.** Plot showing the percentage of germinated and burst grains. Non-germinated PGs were distinguished from germinated PGs by the absence of a detectable PT. **C.** Semi in vivo PT growth showing severe defects in the *lrx8/9* and *lrx8/9/11* mutants compared to the wild type.

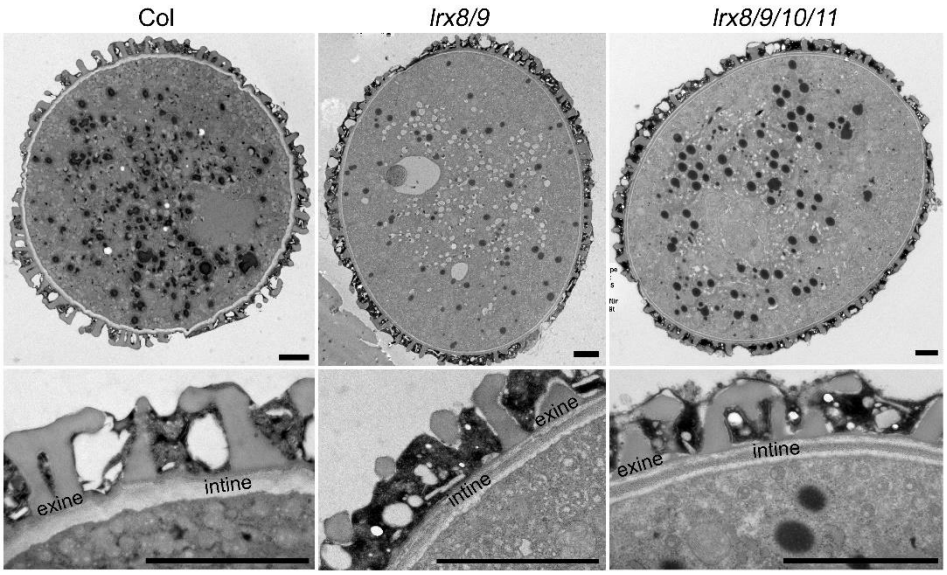

Figure S4: Ultrastructure of pollen grains. Upper panels are full transverse sections through the PGs and lower panels are close-up view showing the pollen wall (intine and exine). A band of electron dense material is seen sandwiched in the intine of *lrx8/9* and *lrx8/9/10/11* mutants, but not in the wild type. Scale bar = 2 µm.

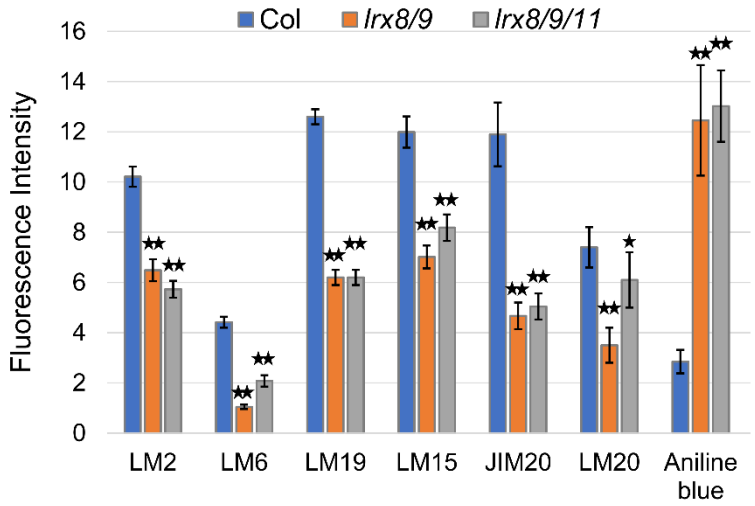

Figure S5: Quantification of immunolabeling cell-wall epitopes. Signal intensity of the different cell wall epitopes indicated in wild-type, *lrx8/9*, and *lrx8/9/11* PTs. Statistics, t-test, * = $p < 0.01$, ** = $p < 0.001$, $n \geq 75$, error bar = s.e.m..

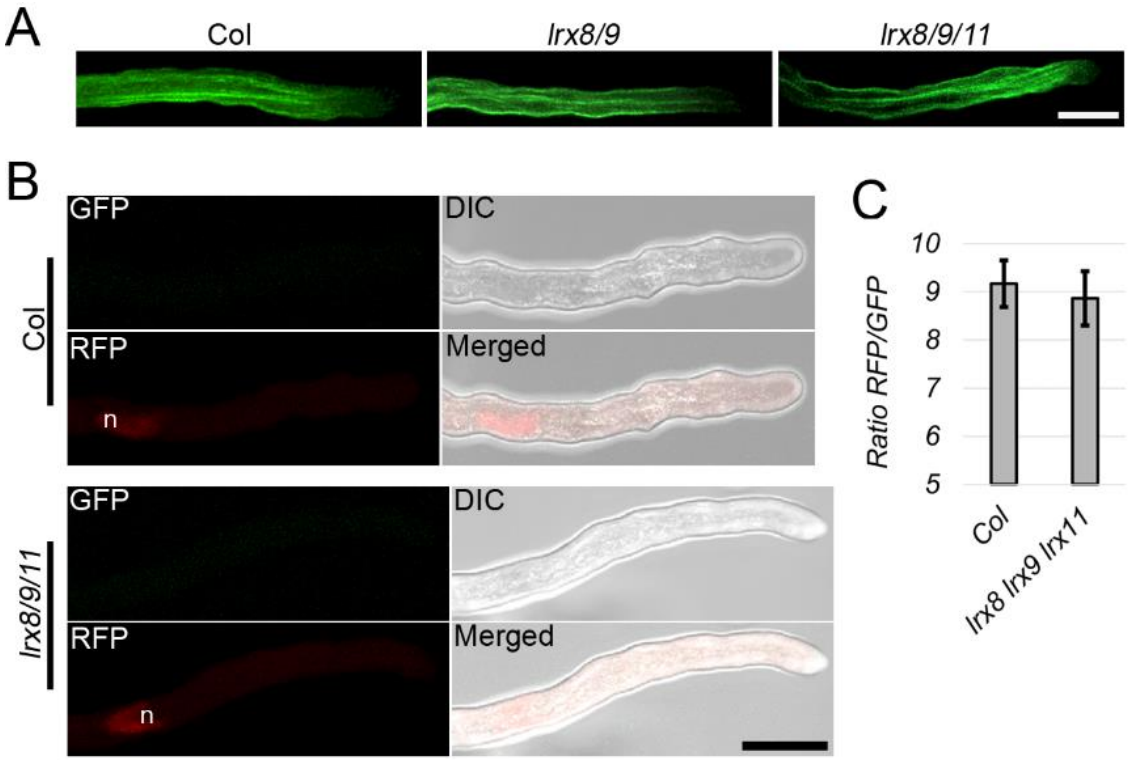

Figure S6: Cytoskeletal organization and cytoplasmic accumulation of secretory vesicles. A. Representative images of the actin filaments showing a similar orientation between wild-type, *lrx8/9*, and *lrx8/9/11* PTs. **B.** Expression of nlsRm-2A-secGf in PTs showing the RFP signal (red) in the nucleus and GFP (almost invisible green) in the cytoplasm, the corresponding DIC and merged images included. **C.** Plot shows comparable ratio of RFP signal in the nucleus to GFP in the cytoplasm. n≥50, error bar = s.e.m., Scale bar = 10 μm.

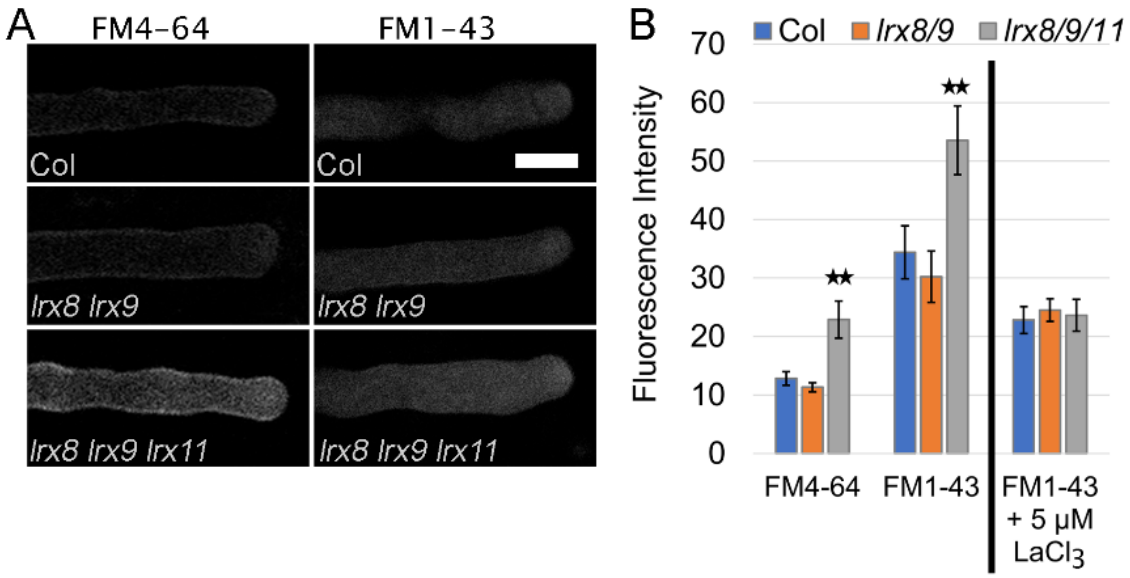

Figure S7: Endocytosis rate in wild-type and *lrx* mutant pollen tubes. A. Representative images of FM4-64 and FM1-43 stained PTs in standard PGM showing higher intensity in *lrx8/9/11* than wild-type and *lrx8/9* PTs. **B.** Plot of the fluorescence intensity for both stains in standard PGM and for FM1-43 in PGM substituted with 5 µM $LaCl_3$. The rate of dye uptake by endocytosis is significantly higher in the *lrx8/9/11* mutant in standard PGM compared to wild-type and *lrx8/9* PTs, but not in PGM substituted with 5 µM $LaCl_3$. Statistics, t-test, ** = $p < 0.001$, n≥50, error bar = s.e.m., Scale bar = 10 µm.

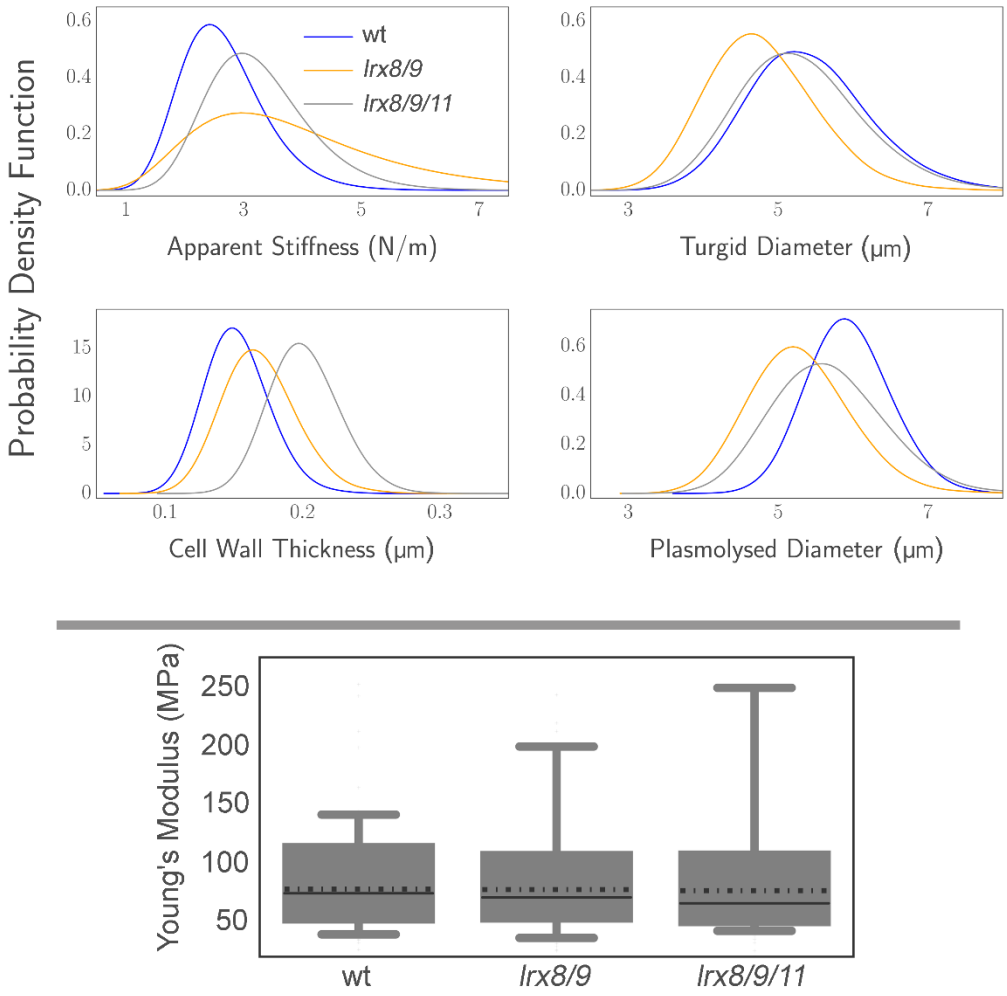

Figure S8: Mechanical properties of wild-type and *lrx* mutant pollen tubes. Top: Input parameters for the FEM model. These include the CFM determined apparent stiffness of the PT, the TEM determined cell wall thickness, and the diameter of turgid and plasmolyzed PTs. These values are shown as probability density functions. **Bottom:** boxplot of the FEM deduced Young's modulus of the cell wall. Interestingly, despite the differences in the cell wall structure between the wild type and *lrx* mutants, the Young's (elastic) modulus does not seem to change significantly. Solid lines: median, dotted lines: mean.